

Benchmarking Concrete Material Models Using the SPH Formulation in LS-DYNA[®]

Brian Terranova¹, Andrew Whittaker², Len Schwer³

¹ Research Engineer, University at Buffalo, 232 Ketter Hall, Buffalo, New York, 14260, U.S. (brt2@buffalo.edu)

² Professor and MCEER Director, Department of Civil, Structural, and Environmental Engineering, University at Buffalo, 212 Ketter Hall, Buffalo, New York, 14260, U.S. (awhittak@buffalo.edu)

³ Schwer Engineering & Consulting Services, 6122 Aaron Court, Windsor, California, 95492, U.S. (Len@schwer.net)

Abstract

A model of a cylinder with a diameter and height of 400 mm was constructed in LS-DYNA using SPH particles to investigate the unconfined, quasi-static behavior of three concrete material models (i.e., MAT016, MAT072R3, and MAT159) in axial compression. Models were also prepared using Lagrangian solid elements and analyzed in axial compression to generate benchmark stress-strain data. Mesh refinement studies were conducted for the SPH cylinder to investigate the effects of particle spacing on predictions of elastic modulus and peak average axial stress. Analysis of the Lagrangian model showed post-peak softening for MAT072R3 and MAT159 and non-softening (i.e., perfectly plastic) behavior for MAT016. The SPH cylinder reasonably recovered the elastic modulus and peak average axial stress of the Lagrangian cylinder for all three material models, but the post-peak behavior predicted using the Lagrangian cylinder was not recovered using the SPH cylinder for material models MAT072R3 and MAT016.

To further investigate the post-peak behavior of MAT072R3 and MAT016, the uniaxial response of a 400 × 400 × 400 mm cube in compression was simulated using the SPH formulation and small magnitudes of lateral confinement. Results were compared with those from analysis of an identical cube built using Lagrangian elements. The SPH cube reasonably recovered the post-peak behavior of the confined Lagrangian cube using MAT072R3 and MAT016 if a lateral confining pressure of between 0.2% and 2% of the average stress at the unconfined, uniaxial compressive strength was imposed.

Introduction

The Smooth Particle Hydrodynamics (SPH) formulation is a Lagrange particle-based method that divides a domain into a set of discrete mass particles that interact over a spatial distance. The spatial distance, known as a smoothing length, uses a smoothed displacement field computed using a kernel function [1]. The SPH formulation allows for very large mesh distortions and is an effective way to combat problems associated with Lagrangian simulations of impact and blast, namely, severe element distortion and negative volume errors. However, the quasi-static behavior of the concrete material models compatible with the SPH formulation (i.e., MAT016, MAT072R3, and MAT159) has not been formally characterized and benchmarked against solutions generated using Lagrangian solid elements: the purpose of this paper.

The quasi-static, uniaxial stress-strain behavior of unconfined concrete with a range of compressive strengths is presented in Figure 1 [2, 3]. All of these stress-strain curves are similar in shape and include a gradual reduction in strength for strains greater than that associated with peak strength: post-peak softening. The strain at peak strength increases as the compressive strength increases, with a value of 0.002 for normal strength concrete. Displacement control (i.e., displacement (strain) is incremented and the force is measured) was used for all of the tests described in Figures 1a and 1b to obtain the descending branches of the stress-strain curves.

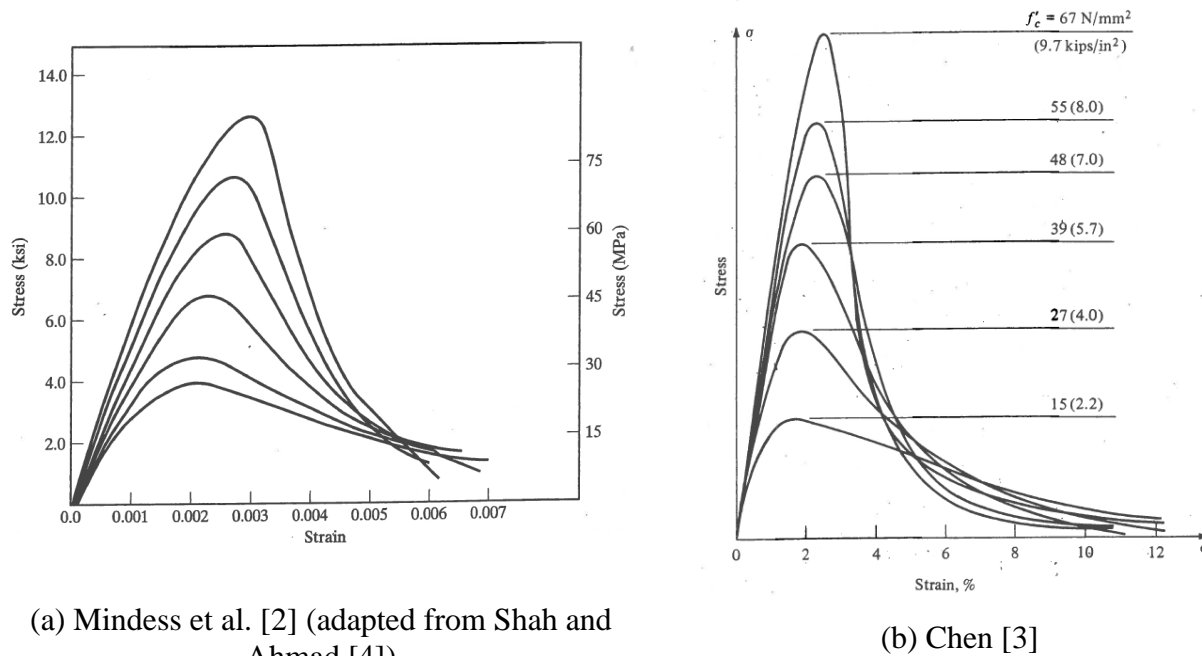


Figure 1: Stress-strain curves for concrete with different uniaxial compressive strengths

Sakakibara et al. [5] investigated the unconfined, quasi-static behavior of an elastic SPH cylinder with a diameter and height of 10 mm using LS-DYNA [6]. The study investigated the effects of particle density (i.e., particle spacing), loading rate, smoothing length, and particle approximation theories on the force-displacement behavior of the cylinder. Results were compared with those of an identical cylinder comprised of Lagrangian solid elements with dimensions of 1 mm \times 1 mm \times 1 mm. The particle density had a significant effect on the predicted stiffness and strength of the material, with both decreasing as the particle spacing increased. A particle spacing of 0.33 mm achieved a force-displacement curve similar to that predicted using the Lagrangian cylinder. Smoothing length values of 1.05 to 1.3 (default is 1.2) were considered; the predicted strength decreased as the smoothing length value increased from 1.05 to 1.3. For the converged particle spacing (=0.33 mm), a value of 1.05 provided a force-displacement curve similar to that predicted using the Lagrangian cylinder. Two particle approximation theories (e.g., default (FORM=0) and renormalization (FORM=1) in *CONTROL_SPH keyword) were investigated using a particle spacing of 0.5 mm. The force-displacement curve predicted using the SPH cylinder was in good agreement with that predicted by analysis of the Lagrangian cylinder using FORM=1. The study conducted by Sakakibara et al. [5] did not investigate other material models available in LS-DYNA compatible with the SPH formulation, such as those for concrete.

The study of Sakakibara et al. [5] prompted the authors to evaluate the unconfined, quasi-static characteristics of the three concrete material models in LS-DYNA compatible with the SPH formulation (i.e., MAT016, MAT072R3, and MAT159) [6] using a model of a cylinder comprised of SPH particles. Models were also prepared using Lagrangian solid elements and analyzed to generate benchmark stress-strain data. Mesh refinement studies were conducted for the SPH cylinder to investigate the effects of particle spacing on the predictions of elastic modulus and peak average axial stress. The results of this study are presented next. Quasi-static simulations of an SPH cube were also conducted for various levels of lateral confinement to further study the characteristics of the concrete models. These results are presented in latter sections of the paper.

Unconfined Cylinder Simulations

A concrete cylinder with a diameter and height of 400 mm (see Figure 2a) was simulated in LS-DYNA using SPH particles to investigate the quasi-static behavior of three concrete material models that are compatible with the SPH formulation. The uniaxial compressive strength of the concrete, *described in units of stress*, was set equal to 45.6 MPa. A Lagrangian model with the same dimensions (see Figure 2b) was created using 40 mm × 40 mm × 40 mm solid elements to benchmark the quasi-static results. The material models considered were MAT016, MAT072R3, and MAT159.

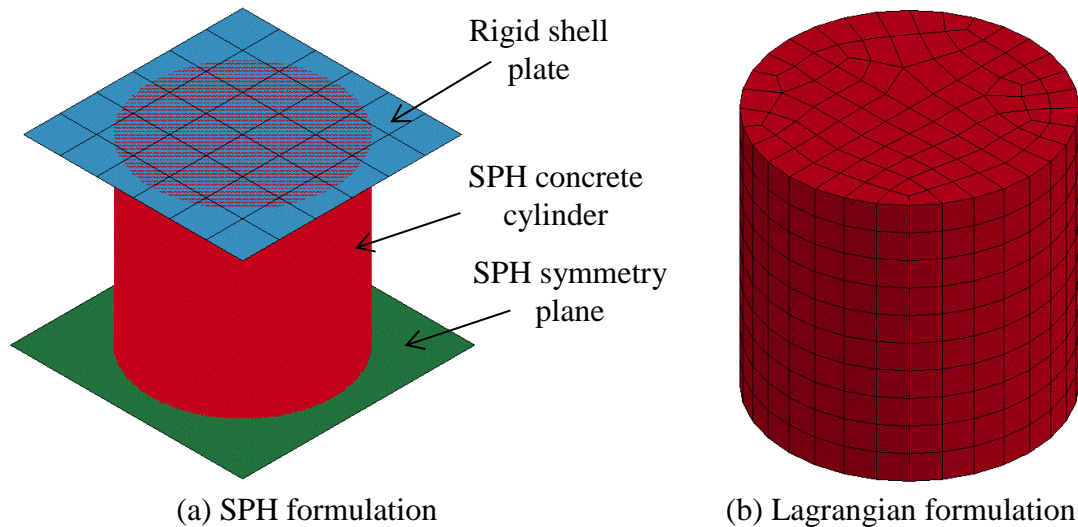


Figure 2: Models of concrete cylinders

The LS-DYNA input parameters are presented in Table 1, where ρ is density, G is shear modulus, ν is Poisson's ratio, and f'_c is concrete compressive strength. An “-” entry in a cell indicates that the parameter is not a required input for the material model.

Table 1: Concrete material inputs

	ρ (g/mm ³)	G (MPa)	ν	f'_c (MPa)
MAT072R3	0.00217	-	0.15	45.6
MAT016	0.00217	4600	0.15	45.6
MAT159	0.00217	-	-	45.6

The Lagrangian cylinder (Figure 2b) was subjected to different rates of loading by applying a constant velocity to all nodes on the top face of the cylinder, corresponding to a specified strain rate. The average axial stress was calculated by dividing the sum of the nodal forces on the bottom face of the cylinder by its cross-sectional area. The SPH cylinder was also subjected to different strain rates by applying a constant velocity to a rigid shell plate (labeled in Figure 2a) that contacts and compresses the concrete cylinder in the axial direction. Contact between the shell elements and the SPH particles (see Figure 2a) was defined using the *CONTACT_NODES_TO_SURFACE keyword. The MST option in the contact keyword, defined as the shell thickness, was set equal to the particle spacing. Simulations were conducted for SPH particle spacing of 4, 8, 16, and 25 mm to identify a converged mesh. The meshes for particle spacing of 4, 8, 16, and 25 mm are presented in Figure 3a through Figure 3d, respectively. The average axial stress was calculated by dividing the sum of the nodal forces on the rigid plate by the area of the cylinder. The boundary conditions at the bottom of the cylinder were created using the keyword *BOUNDARY_SPH_SYMMETRY_PLANE. The default particle

approximation theory (FORM=0 in the *CONTROL_SPH keyword) and the default smoothing length (CSLH=1.2 in *SECTION_SPH keyword) were used for all simulations.

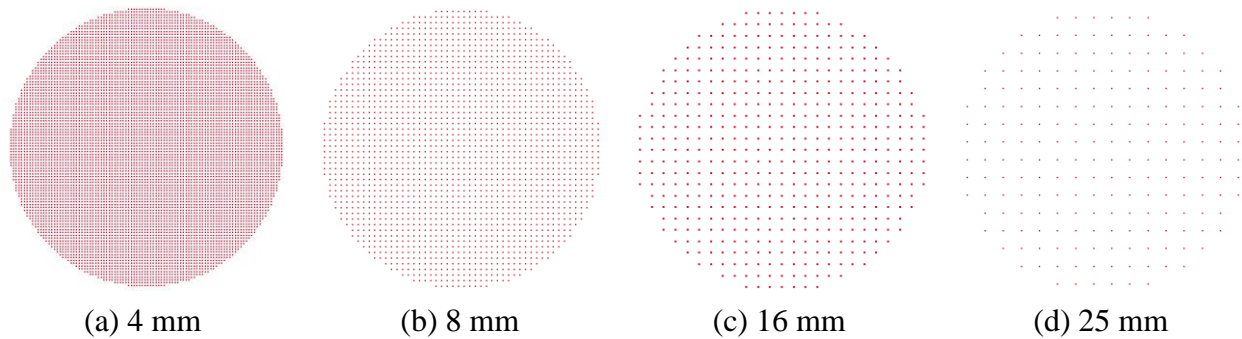


Figure 3: SPH meshes of a 400-mm diameter concrete cylinder

Figure 4, Figure 5, and Figure 6 show the uniaxial stress-strain behavior of the Lagrangian cylinder (see Figure 2b) using concrete material models MAT072R3, MAT016, and MAT159, respectively, at nominal strain rates (SR) of 0.0005/s, 0.005/s, 0.05/s, 0.25/s, and 1/s. The axial stress-strain curves are similar for strain rates of 0.0005/s, 0.005/s, 0.05/s and 0.25/s but response oscillations were observed for a strain rate of 1/s. Since the axial stress-strain behavior at a strain rate of 0.25/s is similar to that at 0.0005/s, which is representative of quasi-static loading, a strain rate of 0.25/s was used to characterize quasi-static behavior for the SPH simulations. (The use of a greater strain rate reduces the computation time.)

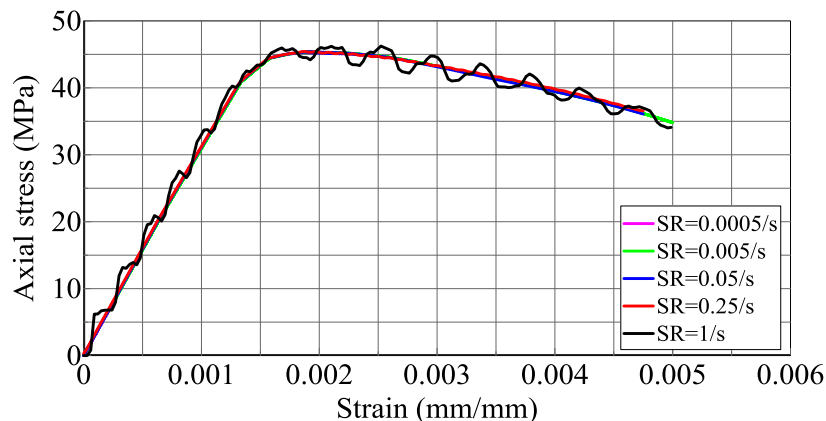


Figure 4: Lagrangian simulations, unconfined concrete cylinder, MAT072R3

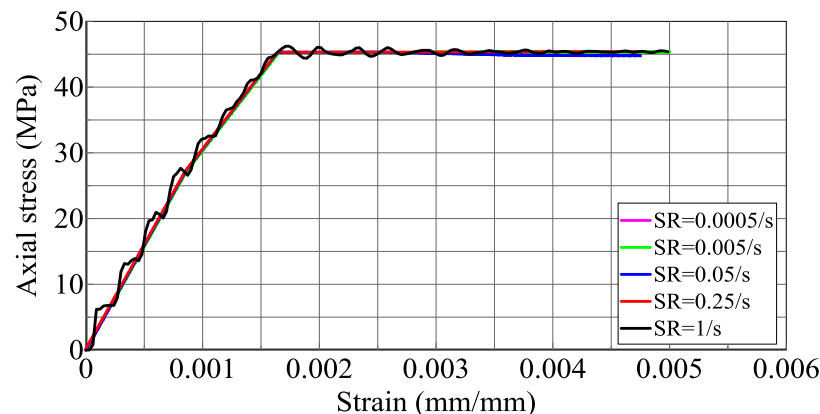


Figure 5: Lagrangian simulations, unconfined concrete cylinder, MAT016

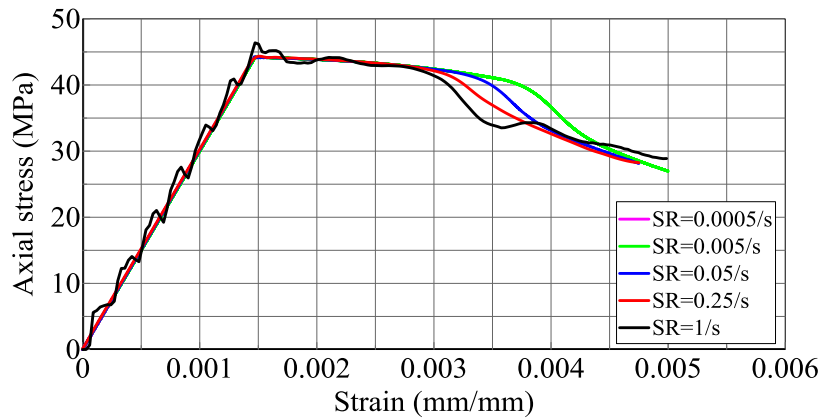
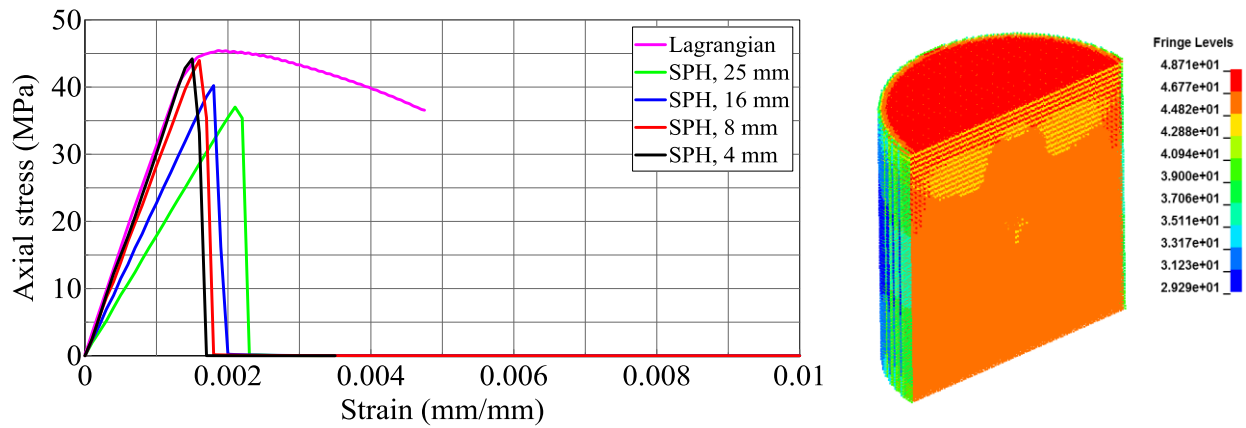


Figure 6: Lagrangian simulations, unconfined concrete cylinder, MAT159

The uniaxial stress-strain behavior of the SPH concrete cylinder using the MAT072R3 material model is shown in Figure 7a, for a strain rate of 0.25/s. The curves are presented for particle spacing of 4, 8, 16, and 25 mm. Results of analysis using a particle spacing of 2 mm were identical to those of the 4 mm mesh, and so 4 mm was assumed to be a converged mesh size.



(a) Stress-strain curves

(b) Von Mises stress, 4 mm

Figure 7: Unconfined concrete cylinder, MAT072R3, SR=0.25/s

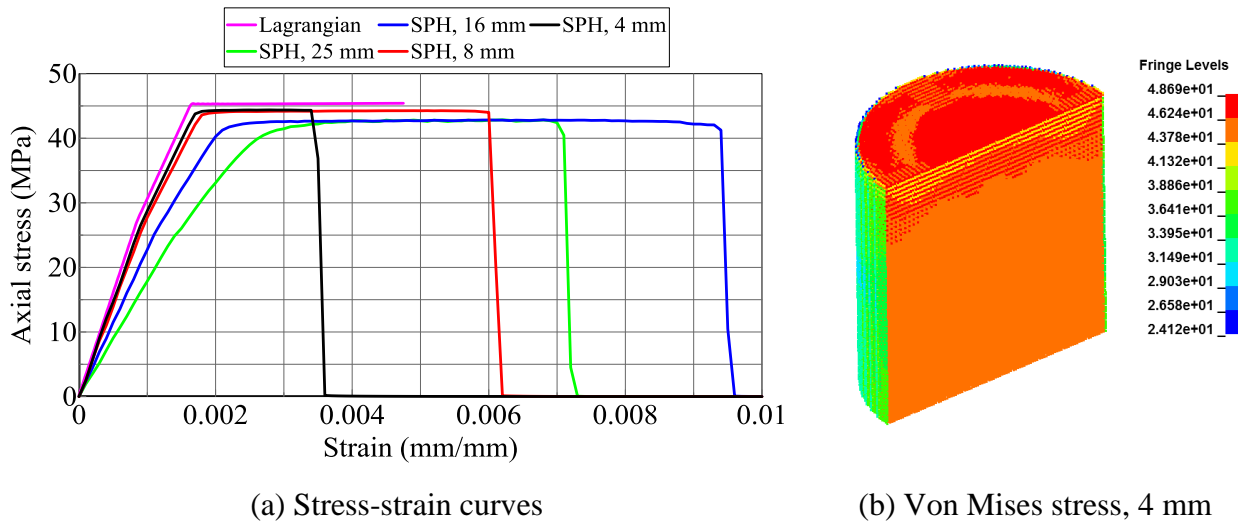
The particle spacing of 4 and 8 mm reasonably recover the average stress (=45.6 MPa) at the compressive strength and the elastic modulus of the concrete (=32000 MPa). The elastic moduli (peak average stresses) calculated by analysis using the 16 and 25 mm mesh are 20000 MPa (40 MPa) and 16666 MPa (37 MPa), respectively. The underestimation of average stress at compressive strength and elastic modulus using the coarser mesh sizes highlight the effect of particle density on the results of the simulations and of the importance of mesh refinement studies; a similar conclusion was reached in Sakakibara et al. [5]. Another important observation is that average axial stress drops immediately to zero after peak stress is reached, suggesting there is no post-peak softening of the unconfined SPH cylinder using MAT072R3. (The effects of confinement on the stress-strain behavior of MAT072R3 in the SPH formulation are investigated in the next section.) The stress-strain response of an unconfined Lagrangian cylinder is also presented in Figure 7a to enable a comparison of results. Based on the results of the SPH cylinder with the finest mesh (=4 mm), both the SPH and Lagrangian formulations predict similar peak values of average axial stress and elastic moduli, but post-peak softening (seen above in Figure 1) is observed only with the Lagrangian model.

The distribution of von Mises stress in the cylinder with a particle spacing of 4 mm, at time of peak average stress (=6 msec), shown in Figure 7b, is not uniform: the inner core of the cylinder reaches the average stress at compressive strength (=45.6 MPa), the stresses in the particles in contact with the shell elements are slightly greater (=48.7 MPa) than the average stress, and the stresses in the particles on the outer edges of the cylinder (=39 MPa) are less than the average stress.

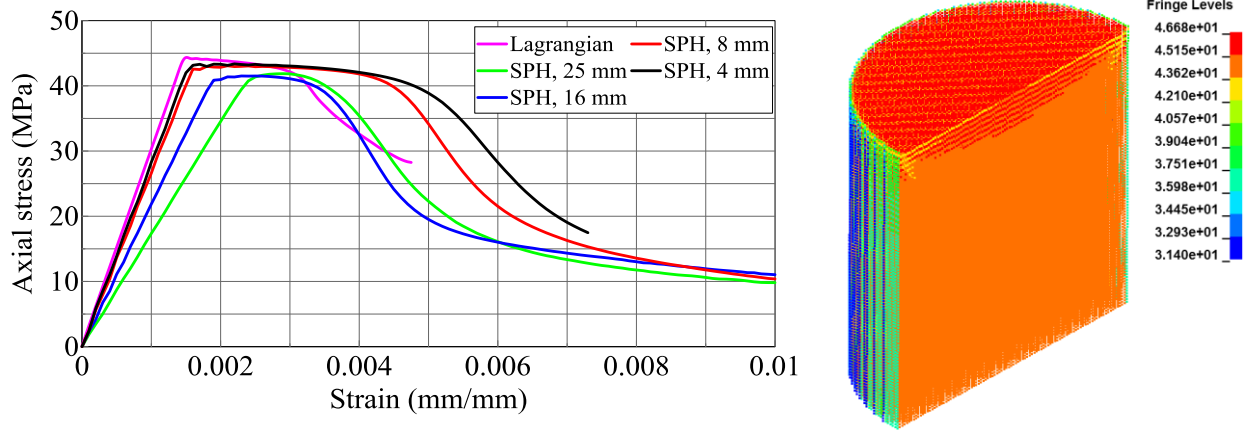
Figure 8a and Figure 9a present the uniaxial stress-strain curves for material models MAT016, and MAT159, respectively, at a strain rate of 0.25/s. The curves are shown for particle spacing of 4, 8, 16, and 25 mm. The stress-strain behavior of the Lagrangian cylinder is also presented in Figure 8a and Figure 9a for MAT016 and MAT159, respectively, for the same strain rate. The simulation results using the 4 and 8 mm mesh reasonably recover the average stress (=45.6 MPa) at peak compressive strength and the elastic modulus (=32000 MPa) for MAT016 and MAT159. Similar to the results of the simulations using MAT072R3 (Figure 7a), analyses using the 16 and 25 mm meshes underestimate the average stress at the peak compressive strength and the elastic modulus. The material model MAT159 exhibits post-peak softening, similar to that predicted using the Lagrangian cylinder, whereas MAT016 exhibits non-softening (i.e., perfectly plastic) behavior, and the average stress drops to zero at a *failure* strain. The *failure* strain for MAT016 is strongly dependent on the particle density in the unconfined cylinder and is not a user-defined input for this material model.

The distribution of von Mises stresses in the SPH cylinders at time of peak average stress is presented in Figure 8b and Figure 9b for MAT016 and MAT159, respectively. Similar to MAT072R3, a relatively uniform distribution of von Mises stress is observed in the core of the cylinder using MAT016 and MAT159, but the stresses in the particles on the outer perimeter of the cylinder and directly in contact with the rigid plate are smaller and greater than the average value, respectively.

The uniaxial stress-strain curves for all three material models using the SPH formulation (4 mm particle spacing) are presented in Figure 10. All three material models recover similar values of peak average axial stress and elastic modulus. However, the stress-strain responses are significantly different in the post-peak-stress region: MAT159 softens, MAT072R3 drops to zero stress, and MAT016 exhibits non-softening behavior.



(a) Stress-strain curves (b) Von Mises stress, 4 mm
Figure 8: Unconfined concrete cylinder, MAT016, SR=0.25/s



(a) Stress-strain curves (b) Von Mises stress, 4 mm
 Figure 9: Unconfined concrete cylinder, MAT159, SR=0.25/s

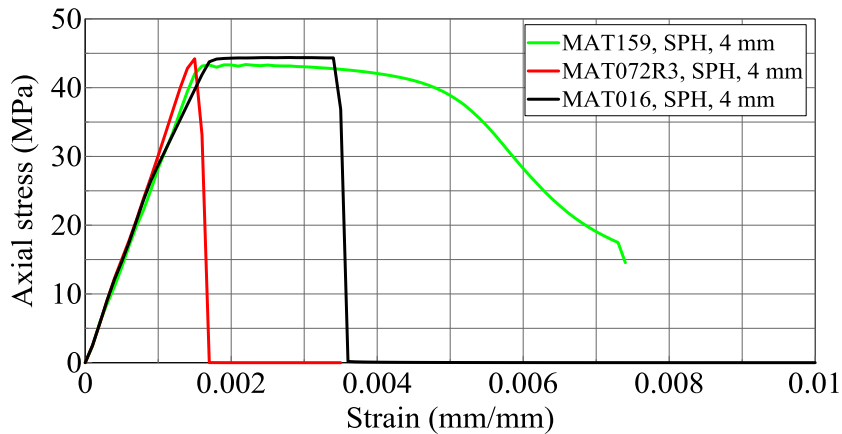


Figure 10: Quasi-static SPH simulations, all concrete models

Confined Cube Simulations

Introduction

The results of the unconfined, quasi-static SPH cylinder simulations presented previously showed: 1) analysis using MAT072R3 predicts an elastic modulus and peak value of average axial stress similar to that of the Lagrangian cylinder, but does not predict the post-peak softening observed in the Lagrangian simulation or in experiments, and 2) the non-softening behavior of MAT016 is similar to that of the Lagrangian cylinder, but the average stress in the SPH cylinder drops immediately to zero at a *failure* strain: behavior not observed in the Lagrangian simulation. The SPH formulation suffers from tensile instabilities (e.g., formation of voids [7]) and this is likely the cause of the differences in response of the SPH and Lagrangian cylinders using concrete models MAT072R3 and MAT016.

This section investigates the quasi-static behavior of MAT072R3 and MAT016 for small magnitudes of lateral confinement (on the order of 0.2% to 2% of the average stress at the unconfined, uniaxial compressive strength (=45.6 MPa)). The goals are to overcome the tensile instabilities of the SPH formulation observed in the unconfined simulations and to recover the stress-strain behavior of the Lagrangian cylinder using the SPH cylinder at very low levels of confinement. A 400 mm × 400 mm × 400 mm concrete cube (see Figure 11a) was constructed using SPH particles; it is simpler to impose a confining pressure on a flat surface of particles. A Lagrangian cube with the same dimensions (Figure 11b) was created using 25 mm × 25 mm × 25 mm solid

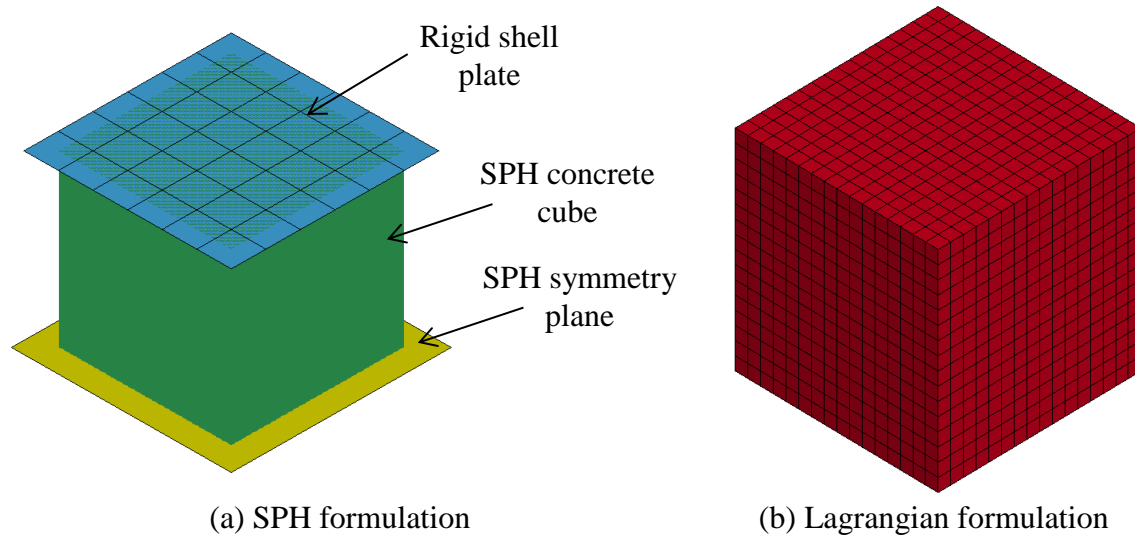


Figure 11: Models of concrete cubes

elements to aid in the comparison of results using the SPH and Lagrangian formulations. The uniaxial concrete compressive strength of the concrete was set equal to 45.6 MPa. The LS-DYNA input parameters for MAT072R3 and MAT016 are those presented in Table 1. The methods used to load the cubes at different strain rates and the calculation of the average axial stresses for the SPH and Lagrangian cubes are similar to those described in the previous section for the unconfined simulations. Contact between the shell elements and SPH particles (see Figure 11a) was defined using the `*CONTACT_NODES_TO_SURFACE` keyword. The `MST` option in the contact keyword, defined as the shell thickness, was set equal to the particle spacing. The keyword `*BOUNDARY_SPH_SYMMETRY_PLANE` was used to create the boundary conditions at the bottom of the cube, as shown in Figure 11a. The default particle approximation theory (`FORM=0` in the `*CONTROL_SPH` keyword) and the default smoothing length (`CSLH=1.2` in `*SECTION_SPH` keyword) were used for all simulations.

Lateral confinement of the SPH cube was applied as follows: 1) the confining pressure was incremented on five faces of the SPH cube (excluding the bottom face where the boundary condition was applied) using the `*LOAD_NODE_SET` keyword until the desired confinement was reached, 2) the stress-state of the cube was saved, and 3) the simulation was restarted from the previous stress state, instantaneously removing the confining pressure from the top face and applying a constant velocity to the rigid shell plate (labeled in Figure 11a) that contacts and compresses the concrete cylinder in the axial direction. The Lagrangian cube was loaded in a similar fashion, but the confining pressure was applied using the `*LOAD_SEGMENT_SET` keyword and was compressed by applying a constant velocity to all nodes on the top face of the cube.

Karagozian and Case (MAT072R3)

The axial stress-strain behavior of the unconfined SPH cube calculated using the MAT072R3 material model is shown in Figure 12, for a strain rate of 0.25/s. The curves are presented for particle spacing of 4, 8, 16, and 25 mm to identify a converged mesh. The unconfined stress-strain behavior of the Lagrangian cube is also presented in Figure 12. Similar to the unconfined cylinder simulations presented in the previous section, results using a mesh spacing of 4 and 8 mm show an elastic modulus and a peak value of average stress similar to that of the Lagrangian cube, but gradual post-peak softening is not predicted. The instantaneous drop from peak average axial stress to zero stress for the SPH simulation of the unconfined cube is also observed for simulations involving small transverse tensile pressures applied to the vertical faces of the model.

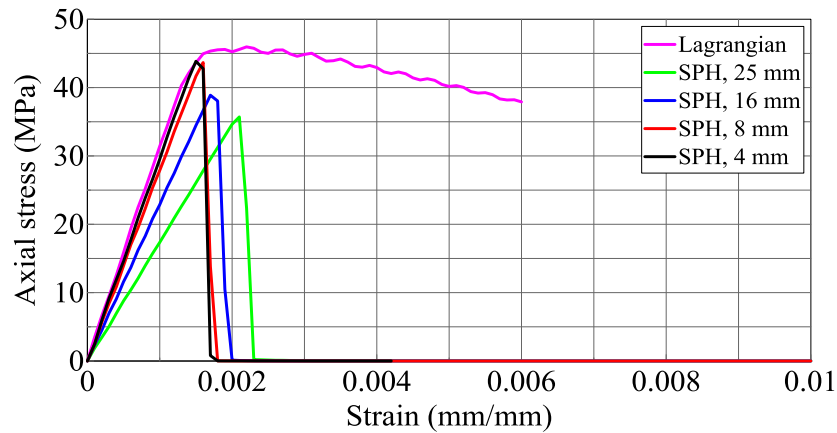


Figure 12: Unconfined concrete cube, MAT072R3, SR=0.25/s

Figure 13 presents the unconfined and confined stress-strain behavior of the Lagrangian cube. Confining pressures of 0.1 MPa, 0.5 MPa, and 1 MPa were considered, which correspond to 0.2%, 1%, and 2% of the average stress at the unconfined, uniaxial compressive strength. The addition of these confining pressures resulted in relatively small changes in peak average stress: stress increases of 1%, 7%, 14% were observed for confining pressures of 0.1 MPa, 0.5 MPa, and 1 MPa, respectively. These increases in peak average stress are expected for frictional materials (i.e., soil and concrete), as a result of the imposed confining pressure.

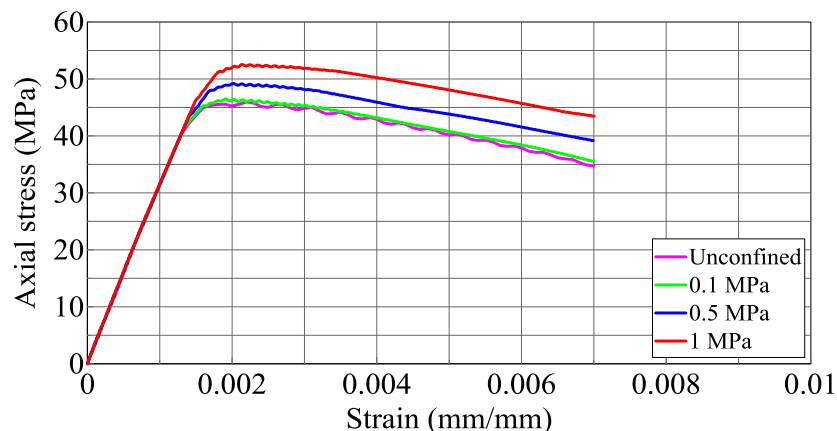


Figure 13: Lagrangian simulations, confined and unconfined concrete cubes, MAT072R3, SR=0.25/s

The stress-strain behavior of the Lagrangian and SPH cubes for confining pressures of 0.1 MPa, 0.5 MPa, and 1 MPa are presented in Figures 14, 15, and 16, respectively. Since analysis with the 4 and 8 mm particle spacing generated similar results in the mesh convergence study (see Figure 12), the cube simulations with the 8 mm particle spacing were used to generate stress-strain curves to reduce the computational effort. For all three levels of confinement considered, analysis of the SPH cube reasonably recovers the elastic modulus, peak value of average stress, and post-peak softening of the confined Lagrangian cube. The results indicate that lateral confinement of 0.2% of the of the average stress at the unconfined, uniaxial compressive strength is sufficient to overcome the tensile instabilities of SPH formulation and for the analysis to predict results similar to that of the Lagrangian simulation using MAT072R3.

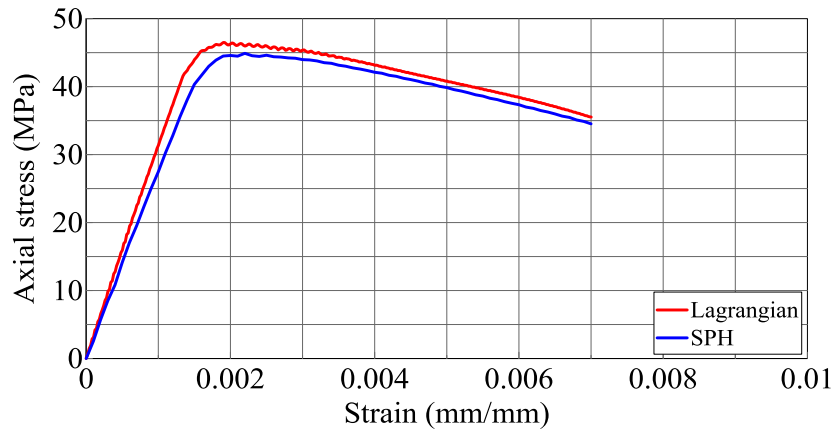


Figure 14: Confined concrete cube, 0.1 MPa confining pressure, MAT072R3, SR=0.25/s

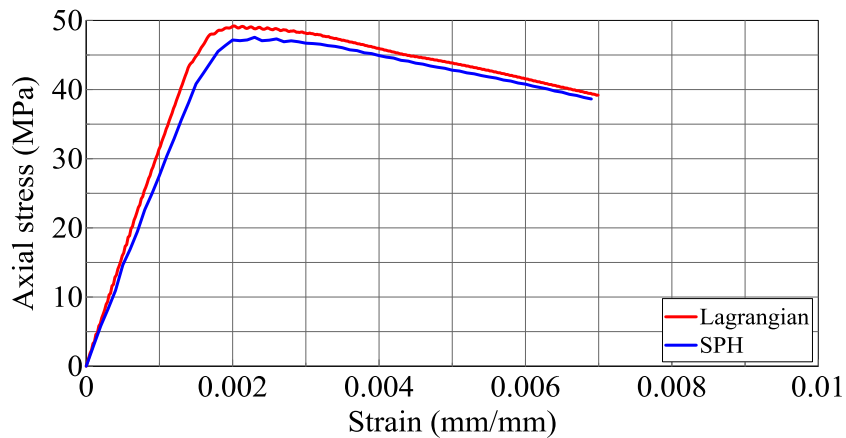


Figure 15: Confined concrete cube, 0.5 MPa confining pressure, MAT072R3, SR=0.25/s

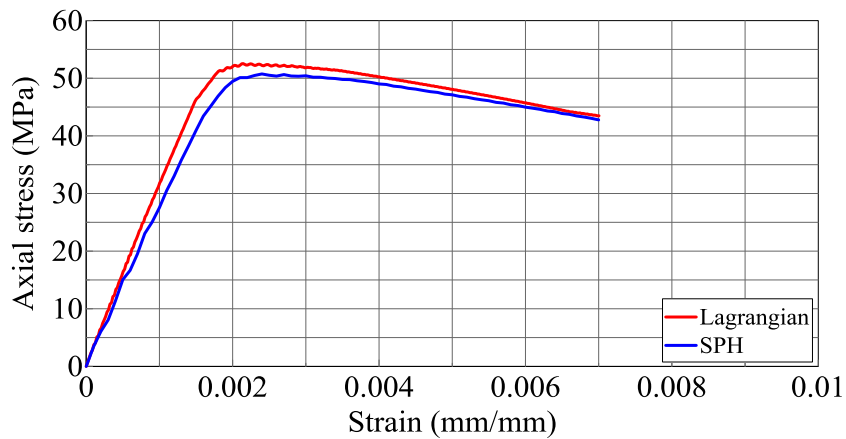


Figure 16: Confined concrete cube, 1 MPa confining pressure, MAT072R3, SR=0.25/s

Pseudo Tensor (MAT016)

Figure 17 shows the unconfined axial stress-strain behavior of the SPH cube using MAT016, for a strain rate of 0.25/s. Results are shown for particle spacing of 4, 8, 16, and 25 mm. The stress-strain behavior of the Lagrangian cube is also presented in Figure 17.

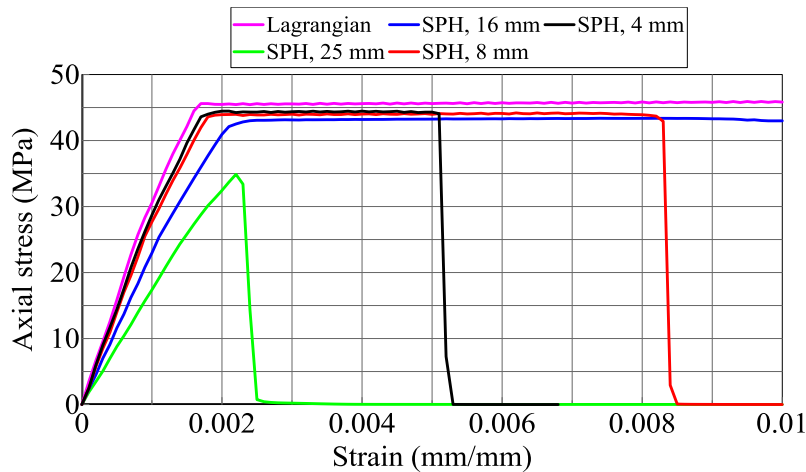


Figure 17: Unconfined concrete cube, MAT016, SR=0.25/s

The 4 and 8 mm particle spacing reasonably recover the elastic modulus and non-softening behavior predicted using the Lagrangian cube, but the *failure* strain in the SPH cube is strongly dependent on the chosen particle spacing; similar behavior was observed in the simulations of the unconfined SPH cylinder presented in the previous section.

The behaviors of the unconfined and confined Lagrangian cubes are presented in Figure 18 for MAT016. Confining pressures of 0.1 MPa, 0.5 MPa, and 1 MPa, corresponding to 0.2%, 1%, and 2% of the average stress at the unconfined, uniaxial compressive strength were imposed. Similar to the Lagrangian simulations of the confined cube using MAT072R3 (see Figure 13), the application of small confining pressures produced small increases in the peak average axial stress.

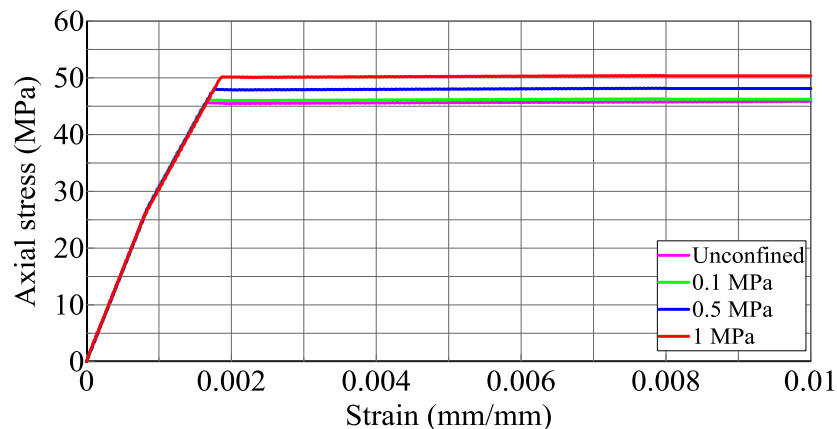


Figure 18: Lagrangian simulations, confined and unconfined concrete cubes, MAT016, SR=0.25/s

Figures 19, 20, and 21 present the stress-strain behavior of the Lagrangian and SPH cubes for confining pressures of 0.1 MPa, 0.5 MPa, and 1 MPa, respectively. The SPH cube reasonably recovers the elastic modulus and peak average axial stress of the Lagrangian cube for all three levels of confinement. As the confining pressure on the SPH cube increases, the value of the *failure* strain increases. For a lateral confining pressure of 2% of the average stress at the unconfined, uniaxial compressive strength of the concrete (=1 MPa), non-softening response similar to that of the Lagrangian cube is obtained.

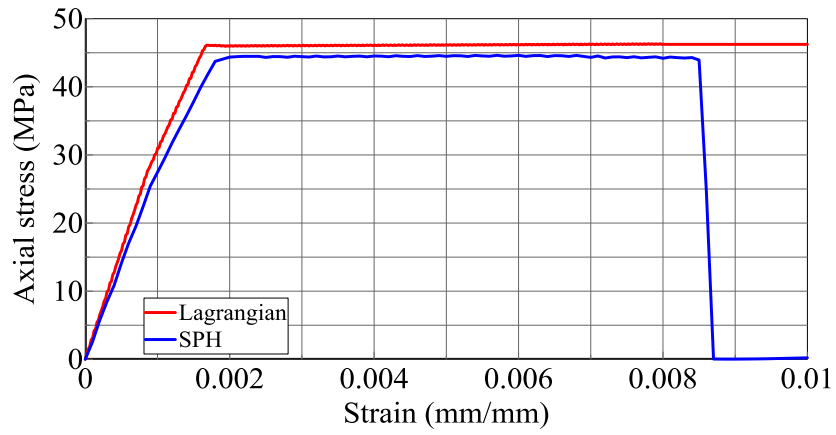


Figure 19: Confined concrete cube, 0.1 MPa confining pressure, MAT016, SR=0.25/s

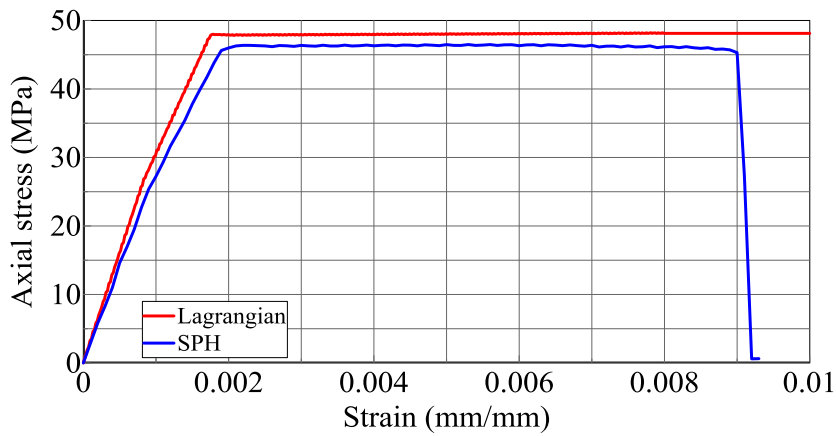


Figure 20: Confined concrete cube, 0.5 MPa confining pressure, MAT016, SR=0.25/s

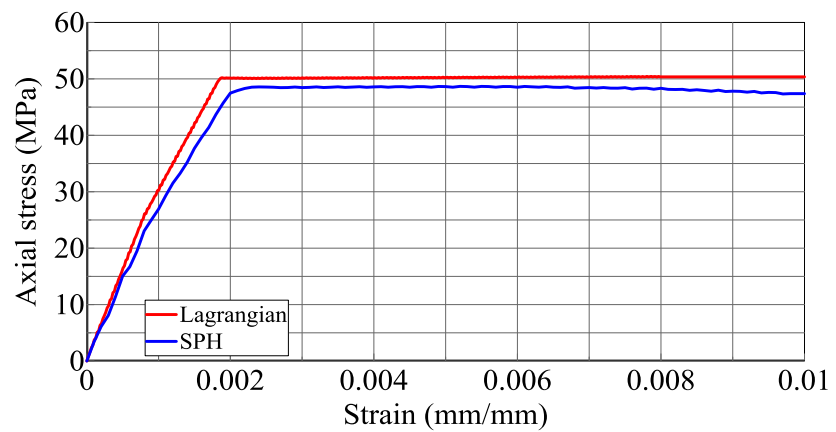


Figure 21: Confined concrete cube, 1 MPa confining pressure, MAT016, SR=0.25/s

Summary and Conclusions

The unconfined, quasi-static behavior of three concrete material models available in LS-DYNA and compatible with the SPH formulation (i.e., MAT016, MAT072R3, and MAT159) were investigated by analysis of an SPH cylinder with a diameter and height of 400 mm. Models were also prepared using Lagrangian solid elements and analyzed to generate benchmark stress-strain data. Mesh refinement studies on the SPH cylinder were performed to investigate the effects of particle spacing on the predictions of elastic modulus and peak average axial stress. Results showed that particle spacing has a significant effect on the predicted values.

Analysis of the Lagrangian model identified the stress-strain response, which included post-peak softening for MAT072R3 and MAT159 and non-softening behavior for MAT016. The SPH cylinder with a 4 mm mesh reasonably recovered the elastic modulus and peak average axial stress of the Lagrangian cylinder for all three material models, but the post-peak behavior predicted using the Lagrangian solid elements was not recovered using the SPH cylinder for MAT072R3 and MAT016.

To further investigate the post-peak behavior of MAT072R3 and MAT016, the behavior of a $400 \times 400 \times 400$ mm cube was simulated using SPH particles and varying degrees of lateral confinement. Mesh refinement studies were performed. Results were compared with those from analysis of a same-size cube built using Lagrangian solid elements. The SPH cube reasonably recovered the post-peak behavior of the confined Lagrangian cube using MAT072R3 and MAT016 with lateral confinement pressure on the order of 0.2% to 2% of the average stress at the unconfined, uniaxial compressive strength.

The findings of this study highlight the importance of benchmarking new codes (i.e., SPH in LS-DYNA) using results from well-established numerical methods (i.e., Lagrangian in LS-DYNA) and from physical experiments.

References

- [1] Lacombe, J.L., (2000). "Smooth particle hydrodynamics (SPH): a new feature in LS-DYNA," *Proceedings, 6th International LS-DYNA Users Conference*, Dearborn, MI, April.
- [2] Mindess, S., Young, J.F., Darwin D. (2003). *Concrete*, Second Edition, Pearson Education, Inc., Upper Saddle River, NJ.
- [3] Chen, W.F. (1982). *Plasticity in Reinforced Concrete*, McGraw-Hill Inc, New York, NY.
- [4] Shah, S.P., Ahmad, S.H. (1985). "Structural properties of high strength concrete and its implications for precast prestressed concrete," *Prestressed Concrete Institute*, 30 (6): 92-119.
- [5] Sakakibara, T., Tsuda, T., and Ohtagaki, R. (2008). "A study of quasi-static problem by SPH method," *Proceedings, 10th International LS-DYNA Users Conference*, Dearborn, MI, June.
- [6] Livermore Software Technology Corporation (LSTC). (2012). *LS-DYNA keyword user's manual V971*, Livermore, CA.
- [7] Mehra, V., CD, S., Mishra, V., and Chaturvedi, S. (2012). "Tensile instability and artificial stresses in impact problems in SPH," *Journal of Physics*, 370 (2012): 1-4.